Carbone *et al. Chem. Biol. Technol. Agric. (2023) 10:134*
https://doi.org/10.1186/s40538-023-00507-3

Chemical and Biological Technologies in Agriculture

RESEARCH

Open Access

Biostimulants promoting growth of *Vicia faba* L. seedlings: inulin coated ZnO nanoparticles

Marilena Carbone[1*†], Silvia De Rossi[2†], Domenica Tommasa Donia[1], Gabriele Di Marco[2], Bianca Gustavino[2], Ludovica Roselli[1], Pietro Tagliatesta[1], Antonella Canini[2] and Angelo Gismondi[2]

Abstract

In the present contribution, inulin coated ZnO nanoparticles (ZnO@inu NPs) were investigated for their potential application on crop production systems, by appraisal of their biostimulating effects on *Vicia faba* L (faba bean). Naked and coated ZnO NPs were synthesized according to purposely implemented eco-friendly protocols and characterized with multiple techniques to determine their crystallographic phase, average particle size, and degree of coating. Faba beans were grown in culture medium supplemented with NPs at 50 or 100 mg kg^{-1}, using ZnO NPs alone, inulin alone, a mixture of the two, or ZnO@inu NPs. Seed germination rate and biometric evaluations on seedlings were carried out, together with Zn localization in the plant tissues. Cellular and molecular effects were ascertained by analyses of photosynthetic pigments, cytotoxicity, genotoxicity, viability, induction of oxidative stress and tissue damage, antioxidant response, and modulation of gene expression. These combined studies indicated a potential role of ZnO@inu NPs in promoting growth and development of *V. faba* seedlings, acting at a post-germinative phase, probably by stimulating the stem cell mitosis. Finally, inulin as a coating agent for the ZnO NPs favored the bioavailability and adsorption of the nanomaterials into the plant tissues, without altering their bioactivity but mitigating any adverse side effect.

Keywords Biotechnology, Sustainability, Crop yield, Phytostimulant, Faba bean

†Marilena Carbone and Silvia De Rossi have equally contributed to the present work.

*Correspondence:
Marilena Carbone
carbone@uniroma2.it
Full list of author information is available at the end of the article

Graphical Abstract

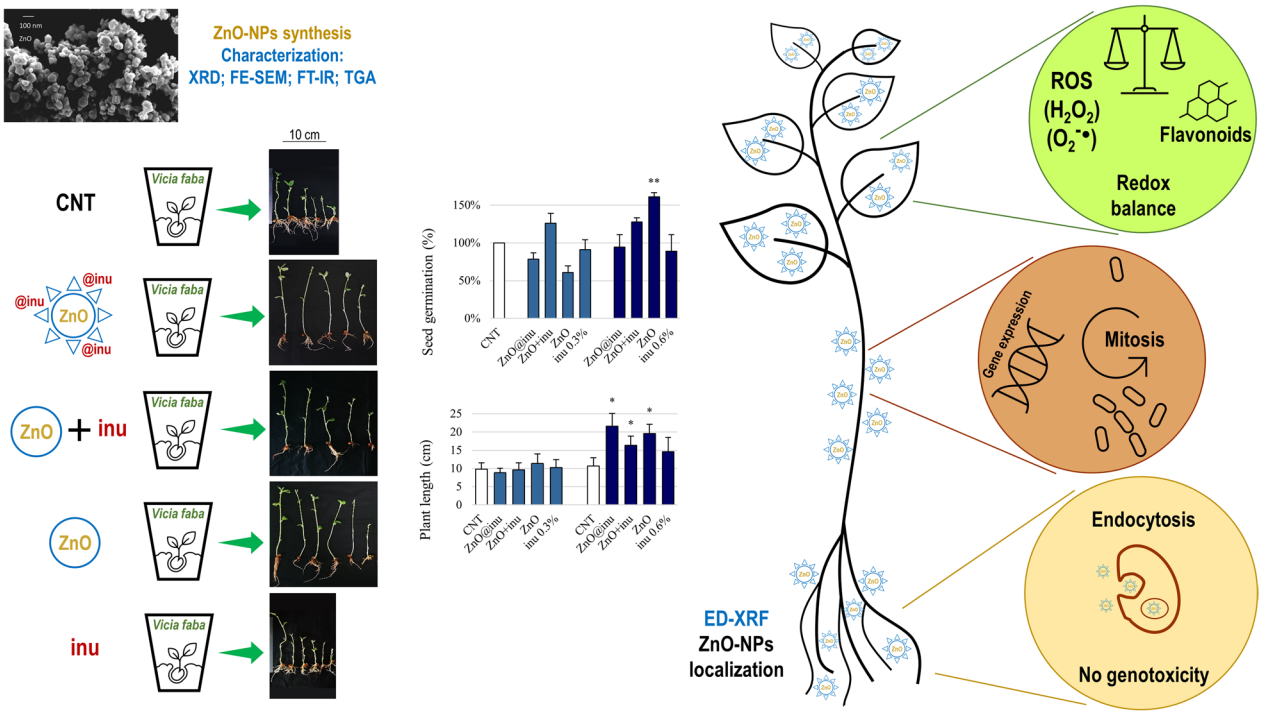

Introduction

"Zero hunger" is one of the ambitious sustainable development goals of the United Nations 2030 Agenda [1]. The challenge of food security in a context of climate change and ever-growing world population should start from a new concept of agriculture. Crop production may largely benefit from the use of biostimulants, i.e., substances, including micro-organisms, that are applied to plant, seeds, soil, or other growing media that may enhance the plant's ability to assimilate the applied nutrients, or provide benefits to plant development [2]. Inorganic biostimulants represent a nanotechnological approach that could find significant application in the food production systems. In this regard, nanoparticles (NPs; at least one dimension ≤ 100 nm) are in the spotlight as possible tools to release micronutrients in soils, control plant pests and diseases, recover soils from contamination, and promote plant growth [3]. The employment of NPs in soil priming, and especially ZnO, has been recently explored as an effective pathway to enhance micronutrient uptake from the soil, acting as carriers of substances, and to increase the crop productivity, promoting yield and quality of the agricultural products [4]. The action mechanisms are generally related to the pH control of the soil, by buffering the effects of $CaCO_3$ present in arid grounds, and to the large bioavailability of these materials, due to their nanosize, which limits the deficiency of Zn as micronutrient [5]. Zinc is a trace element essential for plants, which is involved in a plethora of molecular and cellular functions and processes responsible for their development, reproduction, and signaling [6, 7]. When Zn in soil is scarce, or not bioavailable, plant growth is severely impaired, thus threatening crop yields and quality [8]. Therefore, Zn release in soils by ZnO NPs is potentially a strong asset to face the problem of soil Zn deficiency, a phenomenon characterizing huge areas of arable lands worldwide [9]. ZnO NPs have been documented to be excellent candidates as fertilizer: their small size and high dissolution rate would increase the availability of Zn in the soil and its uptake by plants, making ZnO NPs more suitable and effective than bulk ZnO and conventional Zn salts [10–12]. Furthermore, the utilization of ZnO NPs could have a beneficial side effect in controlling the spread of phytopathogens and related infections thanks to the well-recognized antimicrobial properties of these specific nanomaterials [13]. Despite this encouraging premise, contrasting evidence has been reported in the literature; indeed, in previous investigations both toxic [14–17] and

beneficial effects were reported [18–20] at the expense of ZnO NPs on plants, depending on the selected species, dose, method of administration, etc. Accordingly, the research on the topic is focusing on making ZnO NPs more stable, more biocompatible, and less damaging. In this regard, the functionalization of the nanomaterial surface represents a valid method to increase both performance and effectiveness of NPs, ensuring at the same time a reduced toxicity [21–23]. The choice of coating ZnO for soil administration is crucial both to facilitate their uptake in plants and in terms of dietary safety, as it enters the foodstuff. As reported by Thounaojam and colleagues [24], among all, phytochemicals seem to represent optimal choices as stabilizing agents. In addition, in recent years, several sustainable production procedures have been developed and improved, given the big concern related to climate change, environmental pollution, and risk for human health and natural resources [25–27]. The present study is aimed at investigating the biostimulating effects of coated ZnO NPs, based on three pillars: green production of the NPs, effectiveness, and safety. Therefore, we synthesized coated ZnO NPs by eco-friendly protocols and studied their effects on germination and growth of *Vicia faba* L. (faba bean), a Mediterranean crop species largely employed in the literature [28, 29]. Inulin, a polysaccharide already widely used in food and pharmaceutical industry as a stabilizer and excipient, was chosen as capping agent for some of the ZnO NPs we produced, to evaluate its potential chemical and biological activity as coating for the nanomaterial. Santillàn-Urquiza and colleagues [30] have proven that ZnO NPs coated with inulin resulted better dispersed in water, stable and easily incorporable into dairy products; however, it cannot be excluded that the increased bioavailability would be associated to toxic effects. Therefore, the goals of the current work were: (i) to synthesize Zn-NPs, functionalized or not with inulin, by *green* practices; (ii) to check the bioavailability of the Zn in plants cultivated in presence of our ZnO NPs (coated or not); (iii) to investigate the stimulant property of the NPs on germination and growth of *V. faba* seeds and seedlings, respectively; (iv) to determine the cellular and molecular effects of the ZnO NPs on plant tissues, in terms of content of photosynthetic pigments, genotoxicity, viability, induction of oxidative stress and tissue damage, antioxidant response, and modulation of gene expression; and (v) to ascertain the role of inulin as capping agent for the used NPs.

Materials and methods

Synthesis of the nanoparticles

The synthesis of ZnO NPs functionalized with inulin was carried out in two steps, developed based on previous protocols [31, 32]: first ZnO NPs were synthesized and characterized and then they were coated with inulin (henceforth ZnO@inu). The whole synthetic procedure was carried out according to eco-friendly practices, i.e., using water as solvent and temperatures as close as possible to room temperature, throughout all stages of the reactions [33]. In particular, zinc nitrate hexahydrate ($Zn(NO_3)_2$ 6 H_2O) and sodium hydroxide (NaOH) were purchased from Sigma-Aldrich, while the inulin was purchased from ThermoFisher. All the chemicals were of analytical reagent grade. Solutions and dispersions were prepared with deionized water. The synthesis of ZnO was carried out according to the precipitation reaction here reported:

$$Zn(NO_3)_2 + 2NaOH \xrightarrow{T_P} Zn(OH)_{2(s)}\,, ZnO_{(s)} + 2NaNO_{3(aq)} \xrightarrow{T_D} ZnO_{(s)} + H_2O + 2NaNO_{3(aq)},$$

where T_P and T_D were the temperatures during the precipitation and drying phases, respectively, both set at 40 ℃, which was the lowest value for achieving ZnO without further calcination. More in detail, 500 mL of an aqueous solution of 0.1 M $Zn(NO_3)_2$ was thermalized in an oil bath at 40 ℃ and added to 500 mL of an aqueous solution of 0.1 M NaOH dropwise, under vigorous stirring. The reaction was carried out overnight and the final suspension (FS) was split in two fractions. The first one was centrifuged at 1500 *g* for 10 min and washed once using deionized water. The white precipitate was collected and dried in oven at 40 ℃, overnight. For the capping reaction, a dispersion of inulin (inu) was prepared at 3% (*w/v*) in deionized water and left under stirring for 3 h at the room temperature. ZnO@inu NPs were obtained by adding 125 mL of 3% inulin to the remaining fraction (500 mL) of the FS. This solution was left under stirring overnight at room temperature, centrifuged at 1500 *g* for 10 min, and washed once using deionized water. The white precipitate was dried in oven at 40 ℃. Subsequent characterizations, as reported above, indicated the formation of inulin coated ZnO NPs (i.e., ZnO@inu). Finally, a mechanical mixture of ZnO NPs and pure inulin (ZnO + inu) was prepared in a ratio 1:0.25 (*w/w*).

Characterization of the nanoparticles

The samples were characterized by X-Ray Diffraction (XRD), using an X'Pert PRO XRD instrument (Philips) operating with CuK-Alpha radiation. The surface morphology of the nanoparticles was determined with a Field Emission Scanning Electron Microscope (FE-SEM) SUPRA TM 35 (Carl Zeiss SMT, Oberkochen, Germany) operating at 7 kV and an Energy Dispersive Microanalysis system (EDS/EDX, INCAx-sight, Model:7426, Oxford Instruments) operating at 20 kV. In

addition, infrared spectra of the synthesized nanoparticles were recorded by a Shimadzu Prestige-21 Fourier transform infrared spectroscopy (FT-IR) instrument, equipped with an attenuated total reflectance (ATR) diamond crystal (Specac Golden Gate), in the range of 400–4000 cm^{-1} and at a resolution of 4 cm^{-1}. Thermogravimetric analysis (TGA) was also performed using a Q600 thermobalance instrument, in the presence of a dry N_2 flow (100 mL min^{-1}), with a ramp of 10 K min^{-1} from 300 to 1073 K. To estimate the average number of inulin monomeric units existing around ZnO NPs of 58 nm diameter (as determined by SEM imaging), the following formula was applied:

$$\mathrm{Mass_{inulin}} = \frac{\mathrm{mass_{ZnO\ -\ NPs}}\ \%\ \mathrm{WL_{inulin}}}{\%\ \mathrm{WL_{ZnO\ -\ NPs}}} = 4.6\,10^{-18}$$

Here, $mass_{inulin}$ is the mass of inulin per ZnO nanoparticle; $mass_{ZnO\text{-}NPs}$ is the mass of a ZnO nanoparticle, estimated as equal to 6.2 10^{-16} *g*, characterized by a hexagonal close packed wurtzite structure and a diameter of 58 nm; $\%WL_{inulin}$ is the percentage of weight due to inulin loss; and $\%WL_{ZnO\text{-}NPs}$ is the percentage of weight due to residual ZnO nanoparticles.

Plant material and experimental conditions

Faba bean (*Vicia faba* L.) seeds were obtained from the Botanical Gardens of Rome Tor Vergata. After sterilization with 5% sodium hypochlorite for 15 min, seeds were washed three times and soaked in sterile water in the dark for 24 h at 4 ℃. Sterile Microbox vessels (Micropoli, Milan, Italy) were filled with agarized Murashige and Skoog culture medium (henceforth MS; pH 5.8) for carrying out the plant experiments. In detail, two different concentrations of ZnO NPs were tested: 50 and 100 mg kg^{-1}. Except for the controls (CNT), where MS was pure, four different experimental conditions were considered for each treatment concentration. Specifically, for each of them, MS was supplemented with the respective adequate and corresponding quantities of: (i) functionalized NPs (ZnO@inu); (ii) mixture of ZnO NPs and inu (ZnO + inu); (iii) pure ZnO NPs (ZnO); and (iv) pure inulin (inu). The amount of inulin employed in treatments with ZnO + inu and inu alone corresponds to the equivalent amount of inulin in ZnO@inu, taking into account both the ZnO coverage and the doses of the treatments. In particular, for inu alone, this corresponds to 0.3% and 0.6% weight to be compared to treatments with 50 mg kg^{-1} and 100 mg kg^{-1} NPs, respectively.

A total of 25 Microboxes for each experimental point were arranged and prepared, each one containing five seeds of *V. faba*. The cultures were maintained at 22 ℃ with a 14 h photoperiod (light intensity: 120 µmol m^{-2} s^{-1}) for 21 days. At the end of this interval, seedlings were immediately used for analyses or placed in liquid nitrogen and stored at – 80 ℃.

Seed germination and biometric analysis

Seed germination and plant growth were determined as reported in Di Marco et al. [34]. In detail, for each experimental point, the germination percentage was calculated as the ratio between germinated seeds and total number of sown seeds, multiplied by 100. After 21 days, plants were uprooted, and roots were washed with distilled water; measurements of the total length of the plants were performed manually, using a millimeter precision ruler, and results were reported in cm.

Localization of Zn accumulation

Zn content in leaves and roots was estimated out by X-ray fluorescence (XRF) analysis using an energy dispersive X-ray fluorescence (ED-XRF) spectrometer (SPECTRO XEPOS HE XRF) optimized for heavy elements (max power: 50 W; max voltage: 50 kV). The spectrometer was equipped with a Pd/Co alloy tube. Results were obtained through the "TurboQuant powders and liquid" method (XRF Analyzer Pro software) and the SPECTRO procedure calibration model (a combination of the Fundamental Parameter and Extended Compton scattering model, with a calibration of the mass attenuation coefficient).

Photosynthetic pigment content

The total amount of chlorophyll *a* (Chl *a*), chlorophyll *b* (Chl *b*), and total carotenoid (Car) in the leaves of the samples was assessed spectrophotometrically as described by Lichtenthaler [35]. In particular, the plant material was ground to a fine powder with a mortar and pestle under liquid nitrogen; 30 mg was extracted in 80% (*v*/*v*) acetone for 24 h in the dark at 4 ℃. After centrifugation (3000 *g* for 7 min), the absorbance (Abs) of the supernatants was recorded at 470, 645, and 663 by a UV/Vis spectrophotometer (Varian Cary 50 Bio UV–Vis, The Netherlands). Pigment concentrations were obtained by the application of the following formulas:

$$\mathrm{Chl}\,a\left(\mu\mathrm{gmL^{-1}}\right) = 12.25 * \mathrm{Abs_{663}} - 2.79 * \mathrm{Abs_{645}},$$

$$\mathrm{Chl\ b}\left(\mu\mathrm{g\ mL^{-1}}\right) = 21.50 * \mathrm{Abs_{645}} - 5.10 * \mathrm{Abs_{663}},$$

$$\text{Carotenoids}\left(\mu\text{g mL}^{-1}\right) = \frac{1000 * \text{Abs}_{470} - 1.82 * \text{Chl a} - 85.02 * \text{Chl b}}{198}.$$

The results were expressed as micrograms per 100 mg of fresh plant weight (μg 100 mg^{-1} FW).

Cytotoxicity (Trypan blue staining)

Loss of cell viability was monitored according to the protocol of Duan et al. [36], with some modifications. Briefly, plant tissues were incubated in a solution of 1% (*w/v*) Trypan Blue in phosphate-buffered saline (PBS) for 45 min in the dark. After three washings in PBS, the samples were placed in gentle agitation with 100% ethanol, to completely remove chlorophyll, and finally rehydrated in 50% (*v/v*) glycerol solution. Images were acquired by Epson Perfection V700 Photo system and dark areas were quantified against the total surface, using Fiji/ImageJ software (National Institutes of Health, Bethesda, Maryland, USA); the results were reported as percentage.

Cytogenetic analysis

Concerning cytogenetic analysis, sterilization, and seed sowing were performed as described above (see paragraph 2.3), although the Microboxes were filled exclusively with agarized MS. After 4 days, when the primary roots had reached a length of 2 cm, the root tips were removed, cutting about 5 mm from the distal end, in order to promote the growth of the secondary roots. Simultaneously, seed integuments were removed, and seedlings were placed in plastic basins containing the liquid MS. To keep the cotyledons on the surface of the solution, a plastic grid was used for sustaining the seeds and maintaining only the roots fully immersed in the solution. Seedlings were kept in these conditions in the dark, as reported in the standard protocol for micronuclei analysis, [37] for 4 days before the treatments were carried out. Ten germinated seedlings were used for each experimental point, including negative and positive controls. During the treatment, the whole root systems were immersed in one of the following solutions, according to the case, for 24 and 72 h: (i) ZnO@inu; (ii) ZnO; (iii) inu; and (iv) ZnO + inu. The dose tested for investigating the genotoxicity of nanomaterials and inulin was that equivalent to the maximum exposure investigated in the assays performed in in vitro cultures (i.e., 100 mg kg^{-1}). The maleic hydrazide (Merck), a highly mutagenic herbicide, was employed as positive control (PC) at the concentration of 10^{-4} M in water solution for 4 h, followed by a 20 h recovery time in MS. Negative control (CNT) consisted in exposing roots to the pure MS. After the treatments, secondary roots were excised and fixed in Carnoy solution (acetic acid:ethanol, 25:75, *v:v*) for 30 min; then, they were transferred in a fresh fixing solution and stored overnight at 4 ℃. After Feulgen staining, root tips were squashed onto microscope slides in 45% (*v:v*) acetic acid and permanently mounted in Eukitt (ForLab, Italy). MN frequencies were calculated in 25.000 cells per each experimental point (that is 2.500 cells scored per root tip, using a total of 10 tips per treatment). Only proliferating cell populations were considered for MN frequency analysis, based on the simultaneous analysis of the mitotic index of each studied root tip.

Determination of lipid peroxidation

Lipid peroxidation was evaluated by the thiobarbituric acid method [38], as previously reported in De Rossi et al. [39]. The malondialdehyde (MDA) concentration was determined using the extinction coefficient of 155 mM^{-1} cm^{-1} and expressed as nanomoles per gram of fresh weight of plant material (nmol g^{-1} FW).

Reactive oxygen species (ROS) detection

Nitroblue tetrazolium (NBT) assay was performed to detect superoxide anions in leaves, as described in Wohlgemuth et al. [40], with some modifications. Samples were immersed in a solution containing 2 mM NBT in 20 mM phosphate buffer (pH 6.1) and incubated overnight in the dark. Then, they were moved in distilled water to stop the reaction, placed in 50% (*v/v*) glycerol, and scanned (Epson Perfection V700 Photo) to obtain high-resolution images. Dark-blue spots within the plant tissues marked the presence of superoxide anion, due to the generation of formazan; Fiji/ImageJ software (National Institutes of Health, Bethesda, Maryland, USA) allowed their quantification, as a percentage value, with respect to the total observed area. Hydrogen peroxide was detected in the samples following the method of Rodríguez-Serrano and colleagues [41], using the fluorescent probe 2′,7′-dichlorofluorescein diacetate (DCFH-DA). Plant tissues were incubated in the dark at 37 ℃ for 30 min with 25 μM DCFH-DA in 10 mM tris(hydroxymethyl)aminomethane hydrochloride (Tris–HCl, pH 7.5) buffer. After three washes with the same buffer, samples were placed on microscope slides and observed using a Zeiss Axio Observer 7 fluorescent microscope (Zeiss, Jena, Germany). The acquired images were analyzed by Fiji/ImageJ software (National Institutes of Health, Bethesda, Maryland, USA); intracellular fluorescent area was quantified and expressed as a percentage value compared to the total investigated surface.

Total flavonoid content

The aluminum chloride colorimetric assay was performed for determining total flavonoid levels, according to Di Marco et al. [32]. Briefly, plant material was

powdered under liquid nitrogen with a mortar and pestle, and 200 mg was extracted in 2 mL of methanol for 24 h at 4 ℃. Then, 0.5 mL of plant extract was incubated for 30 min at room temperature with 0.1 mL of 10% aluminum chloride, 0.1 mL of 1 M potassium acetate, 1.5 mL of methanol, and 2.8 mL of distilled water. Finally, the absorbance was measured at 415 nm, using an ELISA microplate reader (Sunrise, Tecan, Austria). Flavonoid levels were estimated using a standard curve of pure quercetin (0–5 mg L^{-1}, $R^2 = 0.9975$) and reported as milligrams of quercetin equivalent per gram of fresh weight (μg QE 100 mg^{-1} FW).

Quantitative real-time PCR (qPCR)

Total RNA was purified exactly as reported by De Rossi et al. [37], starting from 50 mg of powdered plant tissue. Quantity and quality of the extracted RNA were evaluated by a Nanodrop 1000 Spectrophotometer (Thermo Scientific, Wilmington, Delaware, USA), while cDNA synthesis and qPCR analysis were carried out following the protocols reported by Novelli et al. [42]. In detail, the amplifications were carried out by a StepOnePlus Real-Time PCR System (Perkin-Elmer Applied Biosystems) set as follows: (i) initial denaturation at 95 ℃ for 5 min; (ii) 40 cycles of denaturation at 95 ℃ for 1 min, primer annealing at 58 ℃ for 40 s, and extension at 72 ℃ for 40 s; and (iii) production of dissociation curve, from 50 to 95 ℃ (rate: 0.3 ℃/15 s). The amount of each transcript was estimated using the $2^{-\Delta\Delta Ct}$ formula [43], using β-TUBULIN as internal loading control (also GAPDH was tested showing comparable results) and CNT samples as unit. The quantitation method was validated by a ΔCt variation analysis at different template concentrations, as widely described by [43]. The primer sequences used in this paper are reported here: β-TUBULIN CHAIN 4 (TUB; F: 5′-AGGGAAACGAAGACAGCAAG-3′, R: 5′-GCTCGC TAATCCTACCTTTGG-3′ [42];); RBOH D1 NADPH OXIDASE (RBOHD1; F: 5′-CATCAAAACAGCTAA GGACACAG-3′, R: 5′-GTACACAATAGGGAGAGT TGGTAGAC-3′; [42]); CATALASE (CAT; F: 5′-GCGCCT GACAGGCAAGATA-3′, R: 5′-TGCCCAAGAGAACGA TCAGC-3′; [39]); CHALCONE SYNTHASE I (CHS; F: 5′-GCAAGAGAACAAATCTTTCTTTTTTCATAT-3′, R: 5′-CAGAAGCATTTGCAGGGCA-3′; [44]); CYCLIN-DEPENDENT PROTEIN KINASE B 1.1 (CDKB1.1; F: 5′-CTGCTAGAAGCAAGGCTGCATGT-3′, R: 5′-ATG TGGACGGCTTTCATTCTCAA-3′; [45]); CYCLIN-DEPENDENT PROTEIN KINASE D 3.1 (CDKD3.1; F: 5′-TTGAAGAGGCAGTGGCAAGA-3′, R: 5′-CATTGC CAACTTTGTCCTTTCC-3′; [45]).

Statistical analyses

All experiments were repeated at least in triplicate and the results are reported as means ± standard error. Data were subjected to one-way analysis of variance (ANOVA) and the statistical differences were determined by the post hoc lowest standard deviations (LDS) test, using PAST software (p values: $^{*}p < 0.05$; $^{**}p < 0.01$; $^{***}p < 0.001$). For cytogenetic analysis, Mann–Whitney non-parametric test was applied and values of $^{*}p < 0.05$ were considered significant.

Results and discussion

Synthesis and characterization of the NPs

The synthesized nanomaterials were characterized by several techniques, in order to determine their structure, morphology, and level of inulin coating. The X-ray diffraction patterns of the samples are reported in Fig. 1A. For comparison purposes, the reflexes of the pure ZnO NPs are additionally reported from JCPDS card 36–1451, corresponding to a hexagonal close packed wurtzite structure. There is a one-to-one correspondence between the synthesized samples and the reference reflexes, thus indicating the achievement of the state of ZnO. More in detail, reflexes at 2θ = 31.7°, 34.3°, 36.1°, 47.5°, 56.5°, 62.9°, 66.3°, 67.9°, 68.9° 72.5°, 76.9°, 81.3°, and 89.5° were identified as belonging to the (100), (002), (001), (102), (110), (103), (200), (112), and (201) planes, respectively. Notably, the coating of inulin did not affect the cores of the particles, nor segregated into a different phase. As a consequence, no additional peaks appeared and the XRD pattern of ZnO@inu resulted comparable to the uncoated sample of ZnO, as already documented by Bauer et al. [46].

The IR spectra of ZnO and ZnO@inu samples are reported in Fig. 1B. ZnO had the typical steep band, rising from 400 cm^{-1} toward higher frequency values, assigned to Zn–O stretching vibrations.[47, 48] Additional broad bands around 860 cm^{-1} and 3360 cm^{-1} were assigned to -OH vibration and stretching vibration, respectively, and associated with the presence of $Zn(OH)_2$. [47, 48] Adsorbed water molecules also contributed to the high frequency band. The simultaneous lack of reflexes of $Zn(OH)_2$ in the XRD pattern indicated that hydroxide groups were present only in traces on the surface of the ZnO NPs, that is in an amount lower than the XRD detectability threshold (i.e., < 0.5%). Additional shallow bands at 1394 cm^{-1} and 1651 cm^{-1} were attributed to the presence of traces of superficial carbonate groups and/or carboxylic -C=O groups [49], likely the outcome of a carbonation process owing to the CO_2 present in the air, since the synthesis was carried out in an open vessel. The IR spectrum of ZnO@inu showed features typical of both ZnO and inulin and provided information on their interaction. The broad band at 3370 cm^{-1} was due to the

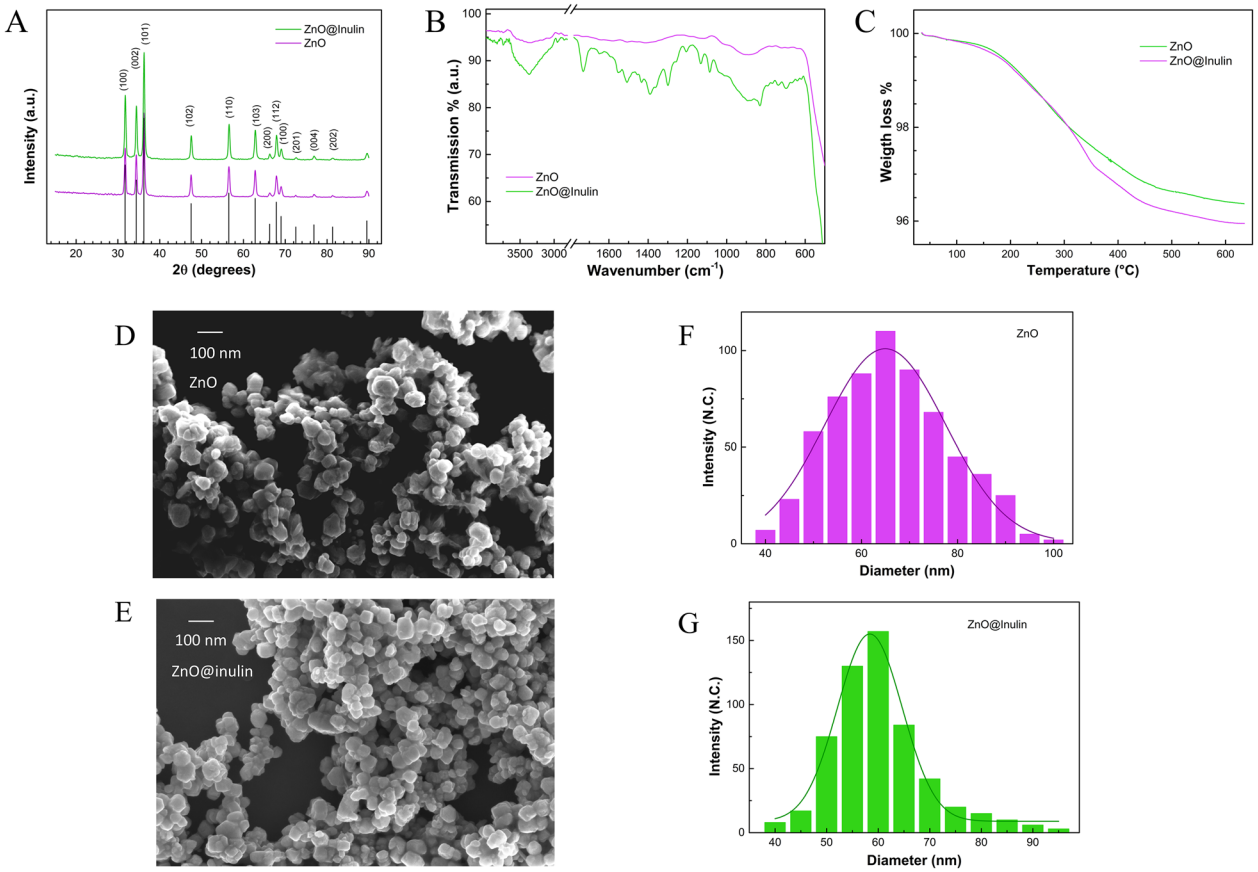

Fig. 1 Characterization of the NPs. **A** XRD powder diffraction pattern of ZnO (—) and ZnO@inu (—); the black vertical lines are the reference data from JCPDS No. 36–1451. **B** IR spectra of ZnO (—) and ZnO@inu (—). **C** Thermogravimetric analysis of ZnO (—) and ZnO@inu (—). SEM images of ZnO (**D**) and ZnO@inu (**E**) and particle diameter distributions of ZnO (**F**) and ZnO@inu (**G**)

-OH stretching vibrations of the inulin and to the residual water. The region between 1400 cm^{-1} and 800 cm^{-1} carried the inulin fingerprints. In particular, the peaks at 1132 cm^{-1}, 1086 cm^{-1}, and 1031 cm^{-1} were representative of the stretching bands of the fructose-furan ring. Peaks at 889 cm^{-1} and 829 cm^{-1} were assigned to anomeric bendings δ(C1–H) and ring vibration of the 2-ketofuranose, respectively, and were indicative of β-(2→1) glycosidic bonds [50]. Bands at lower wavenumbers, in the range between 600 and 800 cm^{-1}, were assigned to -CH_2 rocking vibrations. The typical steep band of ZnO, rising from 400 cm^{-1}, was clearly visible. Bands from 1800 cm^{-1} to 1450 cm^{-1} were related to the presence of carbonyl groups, both free and chelated to Zn. More in detail, the band at 1730 cm^{-1} represented the stretching vibration of a carbonyl group that could be associated to an aliphatic ketone, to an aldehyde, or to an alfa-beta unsaturated ester. Additional bands at 1649 cm^{-1}, 1551 cm^{-1}, and 1508 cm^{-1} were compatible with the chelation of the Zn by two carbonyl groups (e.g., β-diketones), such as in the

Table 1 Identification of IR peaks

Wavenumber (cm^{-1})	Assignment
3370	ν_{O-H} intermolecular H-bonds
1730	$\nu_{C=O\ as}$
1649	$\nu_{C=O-Zn-O=C\ as}$ / δ_{H2O}
1551	$\nu_{C=O-Zn-O=C\ as}$
1508	$\nu_{C=O-Zn-O=C\ as}$
1435	δ_{C-H}
1300	β_{O-H}
1205	β_{O-H}
1132	$\nu_{as\ C-C}$
1086	$\nu_{as\ C-O}$
1037	$\nu_{as\ C-O-C}$
889	Anomeric $\delta_{(C1-H)}$, ring vibration (2-ketofuranose)
829	2-ketose
787-768-696-665-640-619	ρ_{-CH2}
400	$\nu_{as\ Zn-O}$

Infrared bands of ZnO@inu NPs and correlated assignments

case of Zn acetylacetonate [51], and were an indication of the interaction between ZnO and inulin. The presence of residual water might contribute to the band at 1649 cm^{-1}. The infrared bands of ZnO@inu are reported in Table 1 with the correlated assignments.

The thermogravimetric analysis of the samples is reported in Fig. 1C. ZnO displayed a weight loss by 3.6% through the whole temperature range, due to water desorption. ZnO@inu exhibited an additional 0.72% weight loss, compared to ZnO, which corresponded to the inulin coating. This value was used to estimate the average number of inulin monomeric units existing around ZnO NPs of 58 nm diameter, using the formula reported in Materials and Methods section. On average, the analysis indicated 4.6 10^{-18} *g* of inulin per ZnO nanoparticle, that corresponded to 17.700 inulin monomeric units, or 590 polymeric units of 30 monomers each. Morphology and average size of ZnO and ZnO@inu NPs were investigated by SEM microscopy; representative images are reported in Fig. 1D and E, respectively. Both samples were characterized by well-dispersed NPs of rather regular size. An estimation of the average diameter was carried out by statistical analysis of over 600 NPs from 30 images per sample (Fig. 1F and G). According to the size distribution, ZnO and ZnO@inu NPs displayed a diameter of 65 ± 4 nm and 58 ± 1 nm, respectively. The smaller dimensions of the ZnO@inu could be attributed to the disaggregating and size controlling effect of the coating, in association to the longer digestion phase upon inulin addition during the synthesis procedure.

Seed germination and biometric analysis

In general, seed germination was not significantly affected by the treatments at low doses (i.e., 50 mg kg^{-1}) with all NPs. At high doses (i.e., 100 mg kg^{-1}), a significant increase of about 60% compared to the control (CNT) was observed after exposure to ZnO, while no

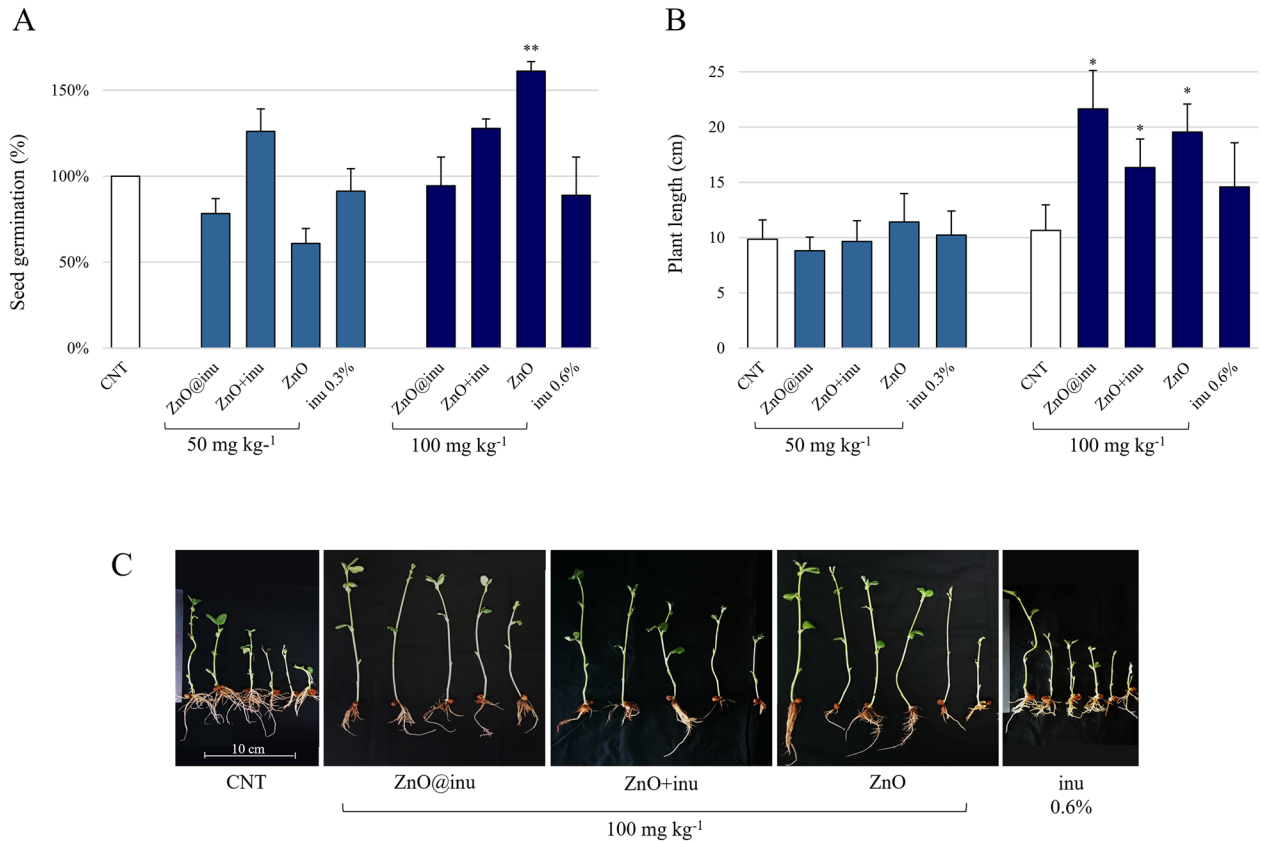

Fig. 2 Seed germination and morphometric analysis. Effects of two concentrations (50 mg kg^{-1} and 100 mg $kg.^{-1}$) of nanomaterials on germination and growth of *Vicia faba*. **A** Germination rates of faba bean seeds in in vitro conditions. The results are expressed as percentage with respect to the control (CNT), considered as unit (100%), and represent the mean ± S.E. of three different experiments. **B** Measurements of the plant length, expressed in cm, of seedlings grown in the presence of the nanomaterials. Data are reported as mean ± S.E. of three independent measurements. **C** Representative images of the samples exposed to the high doses of the several treatments (the scale bar indicates 10 cm). The asterisks denote significant differences of the samples from the respective controls (one-way ANOVA/LSD test; $^{**}p < 0.01$, $^{*}p < 0.05$)

difference could be recorded in the other experimental points (Fig. 2A).

In all cases, pure inulin did not modify the percentage of seed germination. The effect of the NPs on the plant morphology, and in particular on the total length of the seedlings, is reported in Fig. 2B. Also in this case, none of the low-dose treatments produced significant changes in the plant development, compared to the reference control. On the other hand, the plant dimension increased significantly, with respect to the CNT, after all treatments administered in high doses (i.e., ZnO@inu, + 103%; ZnO + inu, + 53%; ZnO, + 84%). Curiously, the inulin alone seemed to have no effect on plant growth, at any of the two tested concentrations. These data may be clearly observed from the images collected in Fig. 2C, where it should be noticed that the stem was the main plant district whose dimension was modulated by the high doses of all NPs. No significant differences could be observed in average number of leaves per plant and root structure and length after the several treatments.

Localization and quantitation of the NPs in the plant tissues

In order to understand if NPs were adsorbed by the seedlings and which was the entity of their accumulation in the plant tissues, ED-XRF analyses were carried out for quantifying the concentration of Zn in the roots and the leaves of *V. faba* grown in the presence of the nanomaterials (Table 2).

Table 2 Localization and quantitation of Zn

Sample/tissue	Zn (ppm)	
	Leaf	Root
CNT	79 ± 1	25 ± 1
ZnO@inu (50 mg kg^{-1})	735 ± 10*	842 ± 10*
ZnO + inu (50 mg kg^{-1})	307 ± 10*	452 ± 5*
ZnO (50 mg kg^{-1})	351 ± 10*	810 ± 10*
inu (0.3%)	332 ± 10*	35 ± 1
ZnO@inu (100 mg kg^{-1})	7190 ± 30*	951 ± 10*
ZnO + inu (100 mg kg^{-1})	2095 ± 15*	153 ± 2*
ZnO (100 mg kg^{-1})	3340 ± 20*	920 ± 10*
inu (0.6%)	1232 ± 10*	37 ± 1

Zn concentration measured in leaves and roots of *V. faba* seedlings exposed to high and low doses of NPs or not (CNT). The results were reported as parts per million (ppm) (*$p < 0.05$ vs CNT)

The Zn content in leaves and roots from the CNT was in line with literature values, [52] whereas it varied significantly depending on the type and dose of treatment. In detail, we observed that Zn level increased both in leaves (min. + 289% with ZnO + inu 50 mg kg^{-1}; max. + 9001% with ZnO@inu 100 mg kg^{-1}) and roots (min. + 512% with ZnO + inu 100 mg kg^{-1}; max. + 3704% ZnO@inu 100 mg kg^{-1}) of all samples exposed to the NPs. However, in all treatments with NPs at low doses (i.e., 50 mg kg^{-1}), a greater accumulation of Zn could be detected at root level, with respect to the respective leaf compartment. On the other hand, the metal was found at higher concentration in the leaves, compared to roots of the same seedlings, when plantlets were cultivated with 100 mg kg^{-1} of nanomaterials. Interestingly, inulin alone (both at 0.3% and 0.6%) induced significant changes of Zn content in the leaves but not in the roots, with respect to the CNT. Thus, considering that only at high doses of treatment with all the NPs we previously observed an increase in dimensions of the seedlings, the concentration of 1232 ppm of Zn (detected in the leaves of *V. faba* exposed to inu 0.6%) can be still considered under the threshold value at which any plant growth variation is induced. Another aspect worthy of note consisted in the fact that the plant tissues exposed to ZnO@inu, in

Table 3 Photosynthetic pigments. Content of chlorophyll *a* (Chl *a*), chlorophyll *b* (Chl *b*), and carotenoids (Car) quantified in seedlings of *Vicia faba* after exposure to low doses (50 mg kg^{-1}) and high doses (100 mg kg^{-1}) of nanomaterials

	Pigments (μg 100 mg^{-1} FW)		
	Chl *a*	Chl *b*	Car
CNT	5.75 ± 0.20	2.10 ± 0.04	1.25 ± 0.03
ZnO@inu 50 mg kg^{-1}	5.65 ± 0.12	1.96 ± 0.02	1.36 ± 0.06
ZnO + inu 50 mg kg^{-1}	4.79 ± 0.41	1.79 ± 0.08*	1.12 ± 0.14
ZnO 50 mg kg^{-1}	6.69 ± 0.30*	2.44 ± 0.14	1.58 ± 0.04*
inu 0.3%	6.19 ± 0.09	2.36 ± 0.06	1.41 ± 0.03
CNT	6.03 ± 0.35	2.09 ± 0.18	1.37 ± 0.05
ZnO@inu 100 mg kg^{-1}	7.20 ± 0.10*	2.41 ± 0.03	1.78 ± 0.01*
ZnO + inu 100 mg kg^{-1}	5.95 ± 0.16	1.98 ± 0.03	1.49 ± 0.06
ZnO 100 mg kg^{-1}	6.43 ± 0.53	2.23 ± 0.15	1.58 ± 0.14
inu 0.6%	6.71 ± 0.34	2.57 ± 0.15	1.66 ± 0.08*

The values are means ± S.E. of three independent measurements. (*$p < 0.05$ vs CNT)

all cases, presented a higher amount of Zn than those treated with ZnO or ZnO + inu.

Photosynthetic pigment content

The total amount of Chl *a*, Chl *b*, and Car in *V. faba* plants was detected spectrophotometrically to evaluate possible alterations at the expense of the photosynthetic machinery due to the presence of the several NPs in the growth medium. As reported in Table 3, the values obtained were generally comparable to those of the controls, both at low and high dose of treatments, with some exceptions.

In particular, at the lowest NP concentration, ZnO alone determined an increase in Chl *a* and Car by 16 and 27%, respectively, compared to CNT. By contrast, when ZnO was administered in combination with inulin (i.e., ZnO + inu), a reduction of Chl *b* content could be observed (-15%). High doses of ZnO@inu promoted an increment in Chl *a* and Car (+ 19% and + 30%, respectively). In addition, an increase in Car (+ 22%) was also recorded in samples grown in the presence of high dose of inulin alone, compared to the control.

Cytotoxicity and genotoxicity of the NPs

The Trypan Blue staining allowed the quantification of the necrotic/dead portions of the tissues from faba bean plants exposed to the different concentrations of NPs (Fig. 3A and B).

No significant differences were observed between each treatment and respective control, regardless of the dose administered. The maximum cytotoxicity, indeed, reached about the 17% of the total area, a value which could be considered as physiological, taking into account that the CNT showed an 11% of stained tissue. In order to confirm these data and also evaluate the potential genotoxicity of the treatments on plants, the micronuclei (MN) test was performed on the secondary root tips of samples grown in the presence of the highest concentration of nanomaterials (i.e., 100 mg kg^{-1}). The obtained data are reported in Fig. 3C; the positive control (PC), carried out by exposing seedlings to the mutagenic herbicide maleic hydrazide, showed a significant increase of the MN frequency, as expected, demonstrating the sensibility of *V. faba* to mutagenic substances. By contrast, MN frequencies between all treated samples and the negative control (CNT) appeared always comparable, both after 24 h and 72 h of treatment, suggesting the absence of genotoxicity at the expense of the investigated NPs. The validity of this test was confirmed by the estimation of the mitotic indices of each experimental point (Fig. 3D), where no significant differences among the treated samples and the CNT could be recorded, indicating that no relevant cytotoxic effect occurred after exposure to NPs.

Cell damage and oxidative stress evaluation

In Fig. 4A, B, and C, the quantitation of MDA, a marker for lipid peroxidation, respectively, in leaves, stems, and roots of *V. faba* seedlings treated with the various NPs is reported. In samples grown with 50 mg kg^{-1} of nanomaterials, leaves and stems did not show any significant variation of MDA level, except for the leaves exposed to ZnO@inu and ZnO + inu where MDA decreased by 22% after both treatments. Curiously, low doses of inu seemed to induce a reduction of MDA in stems (− 33%). On the other hand, in roots, MDA concentrations were found to be significantly higher than control after every treatment. Concerning the exposure of faba bean seedlings to high doses of nanomaterials, all the treatments determined an increase of MDA content in leaves, with maximum values recorded for ZnO@inu (+ 59%) and ZnO + inu (+ 104%), compared to CNT. This phenomenon was not observed in stems, except for the samples grown in the presence of pure inulin (+ 25%). In roots, MDA increased significantly with respect to the control only after exposure to high doses of ZnO + inu and inu alone (+ 25% and + 27%, respectively). The presence of oxidative stress in *V. faba* samples exposed to the various treatments at the two different concentrations of NPs was monitored by histochemical staining, in order to quantify the levels of two main intracellular ROS (i.e., superoxide anion and hydrogen peroxide).

As shown in Fig. 4D and E, the presence of superoxide anion did not change significantly in the samples at low doses of treatment compared to the control, except for ZnO@inu where the amount of this radical increased by 86%. On the contrary, high doses of NPs determined a significant accumulation of superoxide anions both in ZnO@inu (+ 71%) and ZnO + inu (+ 108%), with respect

(See figure on next page.)

Fig. 3 Cytotoxicity and genotoxicity tests. **A** Quantitation of the necrotic tissue revealed by Trypan blue staining in *Vicia faba* tissues after exposure to low (50 mg kg^{-1}) and high (100 mg kg^{-1}) doses of nanomaterials. **B** Representative images of faba bean leaves stained by Trypan blue and collected from seedlings exposed to high doses of nanoparticles. **C** MN frequencies measured in samples treated with 100 mg kg^{-1} of NPs for 24 h and 72 h or exposed to negative (CNT) or positive (PC, 10^{-4} M maleic hydrazide, 4 h) control conditions. **D** Mitotic indices of samples (100 mg kg^{-1} of NPs) and relative controls (negative, CNT; positive, PC) treated for 24 h and 72 h. The asterisks denote significant differences of the samples from the control (one-way ANOVA/LSD test; $^{**}p < 0.01$)

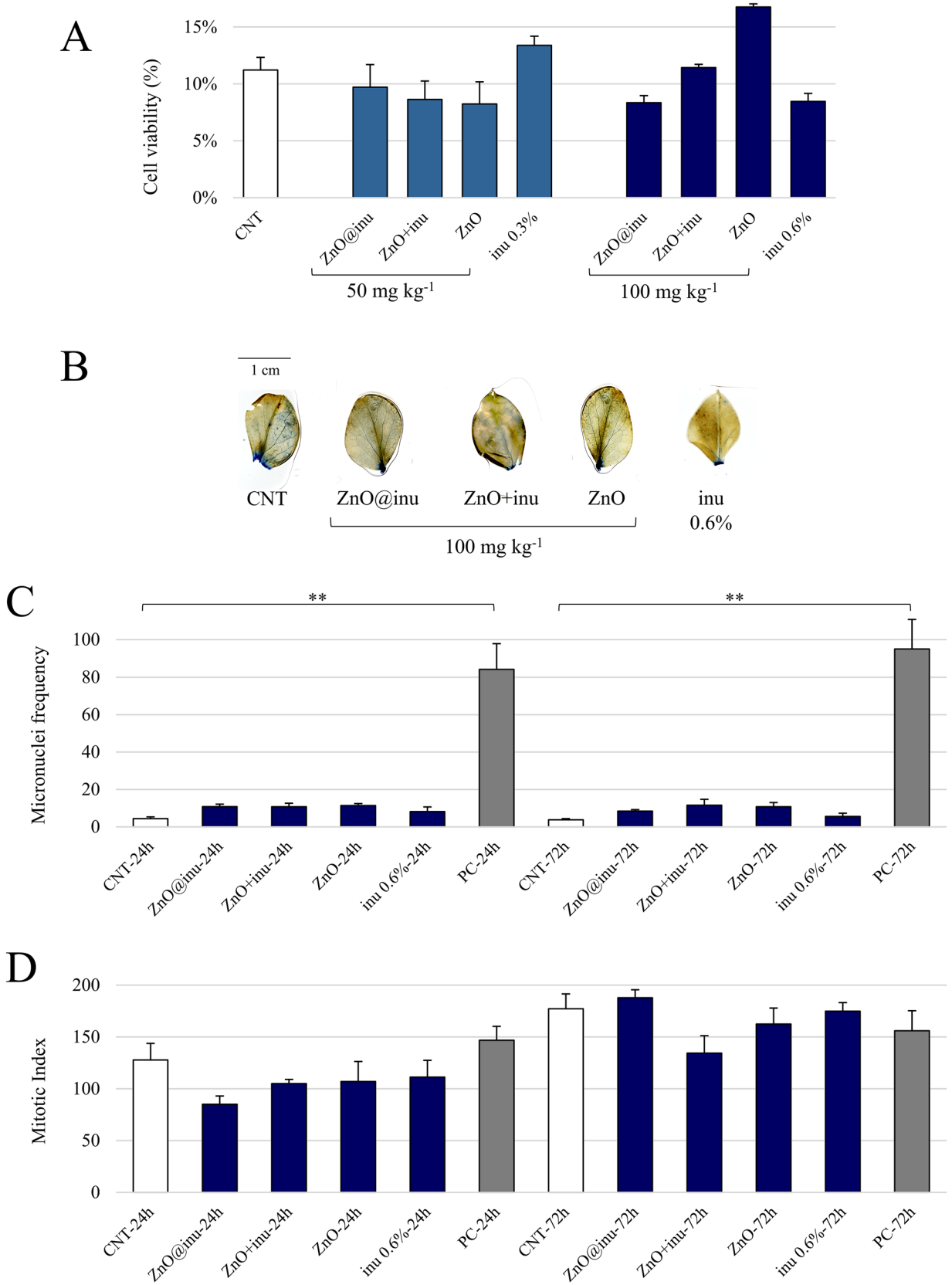

Fig. 3 (See legend on previous page.)

to CNT. Interestingly, hydrogen peroxide content in faba bean samples increased significantly after exposure to all treatments (i.e., ZnO@inu, ZnO + inu, ZnO, inu), both at low and high doses of nanomaterials, except for inu at low doses (Fig. 4F and G). Worthy of note is the fact that the hydrogen peroxide in CNT and inu treatment was mainly accumulated in the apoplast, as clearly visible in the magnifications of Fig. 4G, with respect to the other samples where this ROS could be detected even into the cytoplasm.

Flavonoid content

The concentration of the flavonoids, one of the most important non-enzymatic antioxidant cell systems, was evaluated by spectrophotometric assay, in order to assess the induction of a possible antiradical response of *V. faba* plants to the treatments with the nanomaterials. As shown in Fig. 4H, flavonoids generally tended to increase after exposure to low doses of NPs, and significantly by 49% and 65% compared to the control in the samples ZnO@inu and ZnO + inu, respectively. On the other hand, at high doses, all treatments induced a reduction of the levels for these compounds, particularly registered with ZnO + inu and inu alone (− 47% and − 32%, respectively).

qPCR investigations

To corroborate the previous evidence and/or obtain further data which could help in understanding the molecular mechanisms underlying the bioactivity of the NPs in *V. faba* seedlings, a qPCR analysis was performed on specific cellular targets, which are the following: (i) RBOHD1, a cell membrane respiratory burst NADPH oxidase homolog D enzyme responsible for the production of ROS; [53] (ii) CAT (Catalase), an oxidoreductase which determines the decomposition of hydrogen peroxide to water and oxygen; [54] (iii) CHS (Chalcone synthase), a polyketide synthase that represents the first committed enzyme in flavonoid biosynthesis; [44] and (iv) CDKB1.1 and CDKD3.1, two cyclin-dependent kinases mainly involved in the progression of cell cycle [55]. The analyses were carried out on the samples at high doses and the results are reported in Table 4.

In particular, the mRNA of the plant NADPH oxidase increased significantly after all treatments, as expected. The transcript for the Catalase, interestingly, did not undergo any change, while that of Chalcone synthase tended to remain stable or to decrease, reaching significant peaks in the presence of ZnO + inu and inu (− 28% and − 32%, respectively). Finally, the messenger levels for the two factors inducing cell cycle progression, that is CDKB1.1 and CDKD3.1, resulted up-regulated when treated with all NPs and similar to the CNT after exposure to pure inulin.

Discussion

The "zero hunger" pursuit is challenging and requires a new approach to agricultural methods, where biotechnologies play a pivotal role. A way to sustain the requests of larger food production, for a constantly increasing world population, is ensuring a high ratio of crop yield/seeds. ZnO NPs provide a valuable option for soil priming and increased soil productivity. In addition, several scholars have studied the biological properties of ZnO NPs in human, bacterial, and plant systems. About the latter, the results are quite contrasting and controversial, [56] since each type of these NPs, being synthesized following different methods, can show various bioactivities, depending on several factors, such as their chemical–physical nature, size, shape, possible functionalization, treatment dose, and plant model system on which they are applied.

To date, the employment of coated ZnO NPs for enhancing plant growth has been little explored, though pointing at promising effects. For instance, investigations performed on proline coated ZnO as nanofertilizer have indicated stress alleviating effects [57]. Here, we explored the effects of a polysaccharide capping, represented by inulin molecules, naturally abundant in chicory (*Cichorium intybus* L.) and agave (*Agave* sp. L.), for improving ZnO NPs uptake in *V. faba* (faba bean) seedlings, by mimicking the distribution of a natural substance in the plant. More in general, in this contribution we aimed at

(See figure on next page.)

Fig. 4 Estimation of cell damage and oxidative stress. Quantitation of cell damage and oxidative markers in *Vicia faba* tissues collected from seedlings exposed to two different concentrations of nanomaterials (50 mg kg^{-1} and 100 mg kg^{-1}). Change of lipid peroxidation rate, in terms of MDA content, in leaves (**A**), stems (**B**), and roots (**C**) from samples exposed to low and high dose of nanoparticles. **D** Level of superoxide anion in *V. faba* samples treated with high and low doses of NPs. **E** Representative images of *V. faba* leaves subjected to in vivo localization for $O_2^{\bullet -}$ by histochemical staining with NBT. **F** Hydrogen peroxide levels in samples exposed to low and high doses of NPs. **G** Representative images of *V. faba* leaf portions subjected to in vivo localization for H_2O_2 by histochemical staining with DCFH-DA (the scale bar indicates 20 µm). Magnifications of the areas selected in red are shown. **H** Flavonoid content in faba bean samples treated with low and high doses of NPs. All data represent means ± S.E. of at least three different measurements. The asterisks denote significant differences between samples and respective controls (one-way ANOVA/LSD test; ***$p < 0.001$, **$p < 0.01$, *$p < 0.05$)

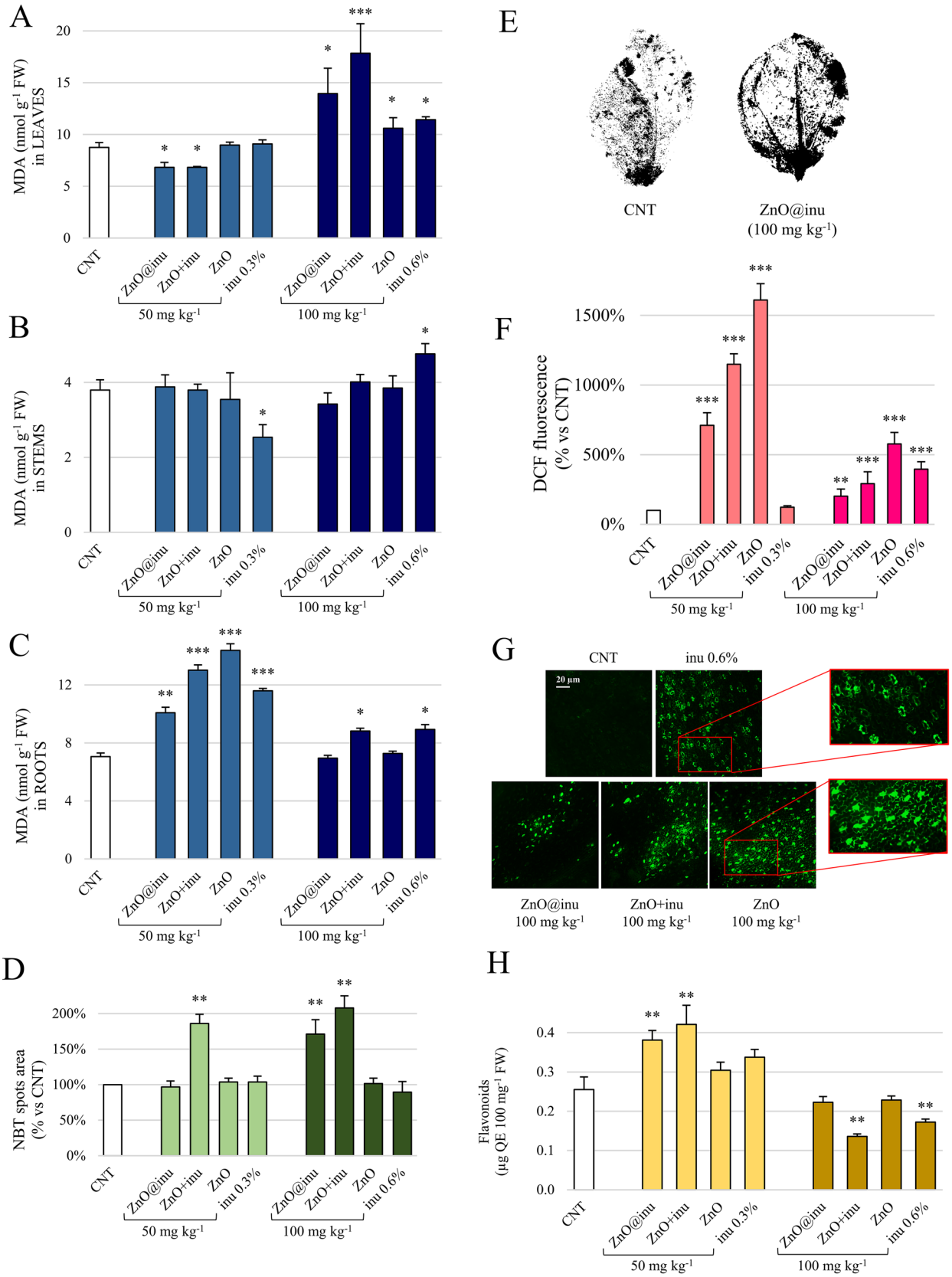

Fig. 4 (See legend on previous page.)

Table 4 qPCR results. Effect of the treatments on the expression of RBOHD1, CAT, CHS, CDKB1.1, and CDKD3.1 genes in *V. faba*. The transcript levels were normalized with respect to β-TUBULIN and expressed in arbitrary units (A.U.) with respect to the control (considered as unit, 1). Data are means ± S.E. of three different measurements (n = 3). (*p < 0.05, **$p < 0.01$; vs CNT)

	Relative transcript level (A.U.)				
	RBOHD1	**CAT**	**CHS**	**CDKB1.1**	**CDKD3.1**
CNT	1	1	1	1	1
ZnO@inu 100 mg kg^{-1}	2.62 ± 0.18**	0.98 ± 0.02	0.92 ± 0.04	1.95 ± 0.13**	1.83 ± 0.19*
ZnO + inu 100 mg kg^{-1}	2.58 ± 0.20**	1.09 ± 0.04	0.72 ± 0.02*	1.76 ± 0.11*	1.80 ± 0.12*
ZnO 100 mg kg^{-1}	3.25 ± 0.22**	0.97 ± 0.04	0.96 ± 0.04	1.88 ± 0.12**	1.72 ± 0.12*
Inu 0.6%	2.73 ± 0.28**	1.03 ± 0.05	0.68 ± 0.03*	0.98 ± 0.04	0.99 ± 0.05

evaluating the effects of ZnO NPs, naked or coated with inulin, on germination and growth of *V. faba*, to understand if such type of nanomaterials may be used as potential plant biostimulants.

In pursuing this goal, we carried out an eco-friendly synthesis of the nanomaterials, fully in aqueous solution. This aspect is very important in terms of sustainability of the production chain and rejection of organic solvents potentially toxic and dangerous to humans and to the environment.

Compared with previously reported synthetic protocols of a similar compound [30], a few differences in the final products need to be mentioned: by our procedure the samples are not contaminated by NaCl and, most important, their average diameter is smaller than that of Santillàn-Urquiza and colleagues [30] (i.e., 58 nm *vs* 92 nm) and with a minimal size dispersion, meaning that the capped NPs have a rather regular shape and size. This property is fundamental when the nanomaterials are administered to the soil since it guarantees a uniform dosing to the plants. Consistently, the weight loss difference we observed between non-capped and capped ZnO NPs is compatible with the coverage of smaller NPs. The IR spectrum of our coated sample revealed the Zn complexation by oxygen atoms, besides the typical inulin features, a type of bond that increases the stability of the capping. Finally, the yield of the synthesis of our NPs is > 95%, hence quite satisfactory.

The treatments with all types of NPs synthesized in this work did not result in cytotoxicity or genotoxicity on the plant samples, regardless of dose. This evidence may suggest a good quality of the tested nanomaterials, that is absence of damaging chemical reactivity, environmental safety, and potential usability in the field. In this regard, it is important to highlight that the doses of NPs used in this study were selected according to the literature, avoiding the ones of 500 mg kg^{-1} that have associated to stress conditions and negative consequences on the rhizosphere [56]. Similarly, others have also indicated that a concentration of ZnO NPs equal to 50 mg/Kg generally determines beneficial effects on plants; [58, 59] therefore, in our research we selected the latter dose in addition to that of 100 mg kg^{-1}, to evaluate whether the bioactivity of the nanomaterials could be dose dependent.

The germination test showed that all treatments did not induce a significant change in the percentage of seed germination, except for the samples exposed to ZnO alone at high doses. In this case, in fact, an increase in the germination rate was observed, suggesting that this compound could somehow promote the development of the sprouts. The hypothesis that can be made is that the naked NPs (may be due to their high concentrations), penetrating through the cracks of the seed coats, favored a major transport of water into the seed, thus promoting the germination mechanism [60, 61]. Indeed, ZnO + inu also seemed to show a similar tendency, while ZnO@inu did not, probably because the functionalized complex was less able to interact with water molecules.

Interestingly, morphometric analyses revealed that the total length (especially relative to the stem) of samples exposed to high doses of all NPs was greater than that observed in the controls. By contrast, no significant change in the content of photosynthetic pigments could be appreciated, suggesting that the photosynthetic machinery was not modified by the treatments and that an increased production of sugars and energy was not the mechanism underlying the observed induction of seedling growth.

The data collected until now would prove a different biological effect of the various studied NPs on faba bean seed germination and seedling growth. These two vital phases are fundamental for plants, and therefore, it

is important to observe how the action of the proposed nanomaterials changed according to their own chemical nature but also to the developmental stage at which they were supplied. However, in general, it could be stated that the low doses of nanomaterials were not perceived by the plant and did not induce any significant effect on seeds/seedlings, while the high concentrations seemed to exert a positive function on them.

Monitoring MDA levels revealed interesting outcomes. Indeed, when exposed to low doses of NPs, *V. faba* seedlings accumulated MDA exclusively in the roots, while in samples grown in the presence of high concentration of nanomaterials significant amounts of MDA were mainly detected in the foliar district. Generally, oxidative stress and consequent cell damage (on lipid molecules) are responsible for MDA accumulation; nevertheless, as stated above, our analyses excluded any toxicity by NP exposure. The peculiar dose-dependent distribution of MDA in the different parts of the plants might be related to the average size of NPs (i.e., 58 nm), which would be excessive for any movement and/or transport via specific carriers and/or protein channels. Indeed, the displacement of NPs of such dimensions would occur by phenomena of endo/exocytosis, [62] implying the remodeling of the plasma membranes with probable damage to its lipid structures, thus resulting in MDA production. In detail, when present at low doses in the growth medium, NPs remained confined to the root level, as demonstrated by ED-XRF analyses, and more precisely where MDA accumulation was observed. By contrast, at high doses, NPs seemed to be able to reach (always by endo-/exocytosis) more easily the vascular bundles (may be due to their elevated concentration) located in the eustele, where their translocation to the aerial parts happened. This would explain the significant presence of MDA in the leaves of the plants treated with high dose of NPs, together with the localization of Zn in the same district. The MDA concentration in the stems from all treated samples (i.e., both at low and high doses) resulted irrelevant, suggesting that the NPs exclusively crossed them, exploiting xylem (and/or phloem), to move from the roots up to the leaves (and vice versa). MDA production as a response to the exposure with inulin alone resulted quite unexpected, considering the plant origin and the natural biocompatibility of this polysaccharide. Unfortunately, literature data about the effects of this fructan on faba bean plants are not available, to clarify this aspect. On the basis of the current evidence, to date, it could be assumed that inulin can somehow cause damage to root cells, perhaps by triggering redox reactions that culminate in an intense lipid peroxidation activity.

It is fascinating to notice that a massive Zn migration toward the leaves was documented in ZnO@inu samples, indicating that probably the inulin coating makes more efficient the internalization and/or the transport of the NPs into the plant tissues. This result would suggest to consider the functionalization with this sugar as a strategy for promoting the bioavailability of other NPs in plants.

In order to better understand whether NPs could induce oxidative stress and ROS accumulation in *V. faba* plant tissues, the concentrations of superoxide anion and hydrogen peroxide were monitored. The levels of superoxide anion did not show a linear trend among the samples, neither at low doses nor at high doses, while hydrogen peroxide always increased significantly after all treatments (except for inu at low doses). This result is not surprising, since it has been reported in the literature that the generation of this reactive species represents the mechanism by which ZnO NPs perform their bioactivity (including the antimicrobial one), thus justifying the constant increase of H_2O_2 with respect to the superoxide anion. Interestingly, it should be noticed that in samples exposed to the lowest doses of NPs the H_2O_2 level was noticeably higher than that measured in plants grown at high doses, suggesting the existence of a hydrogen peroxide accumulation trend inversely proportional to the concentration of the treatment. In this regard, it is essential to point out that the inulin coating (ZnO@inu) did not seem to have a significant role in influencing the variation of superoxide anion concentration, but perhaps only that of H_2O_2 (although further investigation would be necessary to check this hypothesis). Focusing on the effects of the administration of inulin alone, no increase in superoxide anion was registered at both concentrations, while an enhancement of hydrogen peroxide was recorded only after exposure to high doses. In this regard, Boulori et al. [63] have reported how sugars in plants can counteract oxidative stress by acting as ROS scavengers. Indeed, inulin seems able to induce the activity of Catalase and Ascorbate peroxidase, the main enzymes involved in the degradation of hydrogen peroxide [64]. However, as also found for phenolic compounds, [65] it is possible that at high concentrations of inulin can trigger different molecular reactions, thus activating systems for the synthesis of ROS, including hydrogen peroxide. Similar results have been reported by Hashemi and colleagues, [66] who have noticed that ZnO NPs induced an increase in the germination rate of aloe plants (*Aloe vera* (L.) Burm. F.), but at the same time increased lipid peroxidation and production of hydrogen peroxide.

The data relative to the quantitation of flavonoids was of great interest for this study. In fact, an increment of these secondary metabolites was expected after each treatment, at both doses, as an antioxidant response of the plants to mitigate the detected ROS accumulation.

Curiously, the overproduction of these compounds was exclusive for the samples treated with low doses of NPs, while the administration of high doses even seemed to induce a reduction of their synthesis. This evidence, together with the data on the accumulation of ROS (especially hydrogen peroxide) and on the localization of NPs in the plant tissues, suggested for ZnO NPs a peculiar mechanism of action in faba bean seedlings, as here described. At low doses, NPs would remain confined to the root level, where endocytotic uptake would lead to the production of MDA and H_2O_2. To avoid that the redox unbalance induces cell damage and death, antioxidant defense systems would promote the synthesis of flavonoids, highly effective in scavenging ROS (including hydrogen peroxide), inhibiting any cytotoxic effect, which in fact have never been detected in the samples. On the other hand, at high doses, NPs would appear to be more prone to enter the root, maybe by the virtue of their elevated concentration in the culture medium, pushing themselves mechanically into the deepest layers of the cortical parenchyma toward the vascular system. Here, NPs would be distributed throughout the plant, especially toward the apex, where MDA was actually detected. The distribution of NPs throughout the plant is essential to avoid their excessive accumulation in a single site and consequently of H_2O_2. In this case, ROS levels (in particular H_2O_2) would not reach the critical threshold beyond which oxidative stress occurs, saving plants from cytotoxicity and cell death and relieving them from the activation of antioxidant defenses and the synthesis of flavonoids. These observations could even suggest for ROS (e.g., H_2O_2) a different role than the prooxidant one. In fact, it is known that at certain (usually low) concentrations ROS can act as intracellular messenger, capable of stimulating some cellular processes, including cell cycle induction [67]. In addition, even MDA can act as intracellular signal able to stimulate cyclin-dependent kinases (CDKs), proteins responsible for the progression of the cell cycle [68]. Indeed, as reported above, our morphometric analyses revealed a significant growth (at stem level) of the plants treated with high doses of NPs, probably due to the capacity of the latter to confer to the plant cells the ability to proliferate more, or faster, through a ROS/MDA-mediated signaling.

In order to confirm the previous hypothesis, the expression level of specific genes involved in the cell cycle (i.e., CDKs), ROS synthesis (i.e., NADPH oxidase), and ROS enzymatic and non-enzymatic scavenging (i.e., Catalase, Chalcone synthase) were quantified. Interestingly, NADPH oxidase always increased in all samples, justifying—albeit partially—the accumulation of H_2O_2 in the plant tissues. In parallel, despite the presence of high levels of ROS (especially hydrogen peroxide), Catalase and Chalcone synthase showed a tendency to decrease their mRNA, as expected, also considering that flavonoids did not accumulate in the samples exposed to high doses of NPs. Finally, both CDKs were strongly up-regulated after all NP treatments, except for the treatment with inulin alone. All these data support the above-mentioned theory, according to which the main mechanism of action of ZnO NPs, functionalized or not with inulin, would be the promotion of an intracellular signal transduction stimulating plant cell proliferation.

In conclusion, ZnO NPs synthesized and tested in the present study appear to possess a potential biological activity in promoting growth and development of *V. faba* seedlings, acting at a post-germinative phase, likely by stimulating the mitotic activity through a ROS/MDA-dependent molecular signaling. The choice of inulin as a coating agent for the ZnO NPs has favored the bioavailability of these nanomaterials and their adsorption into plant tissues, without altering their bioactivity but mitigating any adverse side effect. Only naked ZnO NPs showed a positive pre-germinative effect, promoting *V. faba* seed germination rate. Further investigations are needed to verify if the produced ZnO NPs can show the same positive effects on other plant species and to continue the molecular analyses able to provide other evidence about the mechanisms underlying the phytostimulant properties of these nanomaterials. However, the data suggest that application of our ZnO NPs, functionalized or not, can represent a promising biotechnology system to be used in the formulation of novel crop cultivation strategies.

Acknowledgements
The present research was funded by University of Rome Tor Vergata, under the grant "Beyond Borders" (Code: E84I20000550005; Principal Investigator: Angelo Gismondi), project title: "Effect of functionalized zinc oxide-based nanoparticles with potential antimicrobial activity on in vitro and in vivo plant model systems (NANOPHYTOTECH)."
Additional funding came from LazioInnova Project "Spectrafood" (Project Number A0375-2020-36643, Code B85F21001350002; Unity Leader: Marilena Carbone) and PRIN2022 "GREEN^3" (Project Number 2022F4YZP9; Principal Investigator: Marilena Carbone).

Author contributions
AG, MC, and BG conceptualized the research; SDR, GDM, DTD, BG, and LR performed the experiments; AG, MC, BG, PT, and AC supervised the research and provided financial support; AG, SDR, MC, and BG wrote the manuscript; all the authors revised the final version of the manuscript.

Availability of data and materials
All the data discussed in this paper are reported in the main text or in the supplementary files associated to the manuscript.

Declarations

Ethics approval and consent to participate
Not applicable.

Consent for publication
Not applicable.

Competing interests
The authors declare no conflict of interest about the present research.

Author details
[1]Department of Chemical Science and Technologies, University of Rome Tor Vergata, Via della Ricerca Scientifica 1, 00133 Rome, Italy. [2]Department of Biology, University of Rome Tor Vergata, Via della Ricerca Scientifica 1, 00133 Rome, Italy.

Received: 20 September 2023 Accepted: 13 November 2023
Published: 22 November 2023

References

1. United Nations General Assembly, Transforming our world: the 2030 Agenda for sustainable development. 2015. https://sdgs.un.org/2030agenda. Accessed 20 Sept 2023
2. Calvo P, Nelson L, Kloepper JW. Agricultural uses of plant biostimulants. Plant Soil. 2014;383:3–41. https://doi.org/10.1007/s11104-014-2131-8.
3. Usman M, Farooq M, Wakeel A, Nawaz A, Cheema SA, Rehman HU, Ashraf I, Sanaullah M. Nanotechnology in agriculture: current status, challenges and future opportunities. Sci Tot Environ. 2020;721:137778. https://doi.org/10.1016/j.scitotenv.2020.137778.
4. Zhang H, Wang R, Chen Z, Cui P, Lu H, Yang Y, Zhang H. The effect of zinc oxide nanoparticles for enhancing rice (*Oryza sativa* L.) yield and quality. Agriculture-London. 2021;11:1247. https://doi.org/10.3390/agriculture11121247.
5. Duhan JS, Kumar R, Kumar N, Kaur P, Nehra K, Duhan S. Nanotechnology: the new perspective in precision agriculture. Biotechn Rep. 2017;15:11. https://doi.org/10.1016/j.btre.2017.03.002.
6. Balafrej H, Bogusz D, Triqui Z-EA, Guedira A, Bendaou N, Smouni A, Fahr M. Zinc hyperaccumulation in plants: a review. Planta. 2020;9(5):562. https://doi.org/10.3390/plants9050562.
7. Hacisalihoglu G. Zinc (Zn): the last nutrient in the alphabet and shedding light on Zn efficiency for the future of crop production under suboptimal Zn. Planta. 2020;9(11):1471. https://doi.org/10.3390/plants9111471.
8. Umair Hassan M, Aamer M, Umer Chattha M, Haiying T, Shahzad B, Barbanti L, Nawaz M, Rasheed A, Afzal A, Liu Y, Guoqin H. The critical role of zinc in plants facing the drought stress. Agriculture. 2020;10(9):396. https://doi.org/10.3390/agriculture10090396.
9. Alloway BJ. Soil factors associated with zinc deficiency in crops and humans. Environ Geochem Health. 2009;31(5):537. https://doi.org/10.1007/s10653-009-9255-4.
10. Beig B, Niazi MBK, Sher F, Jahan Z, Malik US, Khan MD, Pinê Américo-Pinheiro JH, Vo DVN. Nanotechnology-based controlled release of sustainable fertilizers a review. Environ Chem Lett. 2022;20(4):2709. https://doi.org/10.1007/s10311-022-01409-w.
11. Milani N, McLaughlin MJ, Stacey SP, Kirby JK, Hettiarachchi GM, Beak DG, Cornelis G. Dissolution kinetics of macronutrient fertilizers coated with manufactured zinc oxide nanoparticles. J Agr Food Chem. 2012;60(16):3991. https://doi.org/10.1021/jf205191y.
12. Sabir S, Zahoor MA, Waseem M, Siddique MH, Shafique M, Imran M, Hayat S, Malik IR, Muzammil S. Biosynthesis of ZnO nanoparticles using *Bacillus Subtilis*: characterization and nutritive significance for promoting plant growth in *Zea mays* L. Dose-Response. 2020;18(3):1559325820958911. https://doi.org/10.1177/1559325820958911.
13. Tymoszuk A, Wojnarowicz J. Zinc oxide and zinc oxide nanoparticles impact on in vitro germination and seedling growth in *Allium cepa* L.. Materials. 2020;13(12):2784. https://doi.org/10.3390/ma13122784.
14. Ahmed B, Dwivedi S, Abdin MZ, Azam A, Al-Shaeri M, Khan MS, Saquib Q, Al-Khedhairy AA, Musarrat J. Mitochondrial and chromosomal damage induced by oxidative stress in Zn^{2+} ions, ZnO-bulk and ZnO-NPs treated *Allium cepa* roots. Sci Rep. 2017;7(1):40685. https://doi.org/10.1038/srep40685.
15. Alonso-Blázquez N, García-Gómez C, Fernández MD. Influence of Zn-contaminated soils in the antioxidative defence system of wheat (*Triticum aestivum*) and maize (*Zea mays*) at different exposure times: potential use as biomarkers. Ecotoxicology. 2015;24:279. https://doi.org/10.1007/s10646-014-1376-6.
16. Balážová L, Baláž M, Babula P. Zinc oxide nanoparticles damage tobacco BY-2 cells by oxidative stress followed by processes of autophagy and programmed cell death. Nanomaterials. 2020;10(6):1066. https://doi.org/10.3390/nano10061066.
17. Ma H, Williams PL, Diamond SA. Ecotoxicity of manufactured ZnO nanoparticles—a review. Environ Pollut. 2013;172:76. https://doi.org/10.1016/j.envpol.2012.08.011.
18. Ali S, Rizwan M, Noureen S, Anwar S, Ali B, Naveed M, Abd-Allah EF, Alqarawi AA, Ahmad P. Combined use of biochar and zinc oxide nanoparticle foliar spray improved the plant growth and decreased the cadmium accumulation in rice (*Oryza sativa* L.) plant. Environ Sci Pollut R. 2019;26:11288. https://doi.org/10.1007/s11356-019-04554-y.
19. Singh A, Prasad SM, Singh S. mpact of nano ZnO on metabolic attributes and fluorescence kinetics of rice seedling. Environ Nanotech Monit Manag. 2018;9:42. https://doi.org/10.1016/j.enmm.2017.11.006.
20. Sturikova H, Krystofova O, Huska D, Adam V. Zinc, zinc nanoparticles and plants. J Hazard Mater. 2018;349:101. https://doi.org/10.1016/j.jhazmat.2018.01.040.
21. Neouze MA, Schubert U. Surface modification and functionalization of metal and metal oxide nanoparticles by organic ligands. Monatsh Chem. 2008;139:183. https://doi.org/10.1007/s00706-007-0775-2.
22. Subbiah R, Veerapandian M, Yun KS. Nanoparticles: functionalization and multifunctional applications in biomedical sciences. Curr Med Chem. 2010;17(36):4559. https://doi.org/10.2174/092986710794183024.
23. Gulati S, Sachdeva M, Bhasin K K. Capping agents in nanoparticle synthesis: surfactant and solvent system. In: *AIP Conference Proceedings*, *AIP Conf Proc*, 2018; 1: 030214. https://doi.org/10.1063/1.5032549
24. Thounaojam TC, Meetei TT, Devi YB, Panda SK, Upadhyaya H. Zinc oxide nanoparticles (ZnO-NPs): a promising nanoparticle in renovating plant science. Acta Physiol Plan. 2021;43:136. https://doi.org/10.1007/s11738-021-03307-0.
25. Bandeira M, Giovanela M, Roesch-Ely M, Devine DM, da Silva CJ. Green synthesis of zinc oxide nanoparticles: a review of the synthesis methodology and mechanism of formation. Sustain Chem Pharm. 2020;15:100223. https://doi.org/10.1016/j.scp.2020.100223.
26. Kharissova OV, Dias HR, Kharisov BI, Pérez BO, Pérez VMJ. The greener synthesis of nanoparticles. Trends biotechnol. 2013;31(4):240. https://doi.org/10.1016/j.tibtech.2013.01.003.
27. Król A, Pomastowski P, Rafińska K, Railean-Plugaru V, Buszewski B. Zinc oxide nanoparticles: synthesis, antiseptic activity and toxicity mechanism. Adv Coll Inter Sci. 2017;249:37. https://doi.org/10.1016/j.cis.2017.07.033.
28. Leme DM, Marin-Morales MA. *Allium cepa* test in environmental monitoring: a review on its application. Mutat Res/Rev Mutat. 2009;682(1):71. https://doi.org/10.1016/j.mrrev.2009.06.002.
29. Pedruzzi DP, Araujo LO, Falco WF, Machado G, Casagrande GA, Colbeck I, Lawson T, Oliveira SL, Caires AR. ZnO nanoparticles impact on the photosynthetic activity of *Vicia faba*: Effect of particle size and concentration. NanoImpact. 2020;19:100246. https://doi.org/10.1016/j.impact.2020.100246.
30. Santillán-Urquiza E, Arteaga-Cardona F, Hernandez-Herman E, Pacheco-García PF, González-Rodríguez R, Coffer JL, Mendoza-Alvarez ME, Vélez-Ruiz JF, Méndez-Rojas MA. Inulin as a novel biocompatible coating: evaluation of surface affinities toward $CaHPO_4$, α-Fe_2O_3, ZnO, $CaHPO_4$@ZnO and α-Fe_2O_3@ZnO nanoparticles. J Colloid Interf Sci. 2015;460:339. https://doi.org/10.1016/j.jcis.2015.08.057.
31. Carbone M, Briancesco R, Bonadonna L. Antimicrobial power of Cu/Zn mixed oxide nanoparticles to *Escherichia coli*. Environ Nanotechnol Monit Manag. 2017;7:97–102. https://doi.org/10.1016/j.enmm.2017.01.005.
32. Carbone M, Aneggi E, Figueredo F, Susmel S. NiO-nanoflowers decorating a plastic electrode for the non-enzymatic amperometric detection of H_2O_2 in milk: Old issue, new challenge. Food Control. 2022;132:108549. https://doi.org/10.1016/j.foodcont.2021.108549.
33. Donia DT, Bauer EM, Missori M, Roselli L, Cecchetti D, Tagliatesta P, Gontrani L, Carbone M. Room temperature syntheses of ZnO and their structures. Symmetry. 2021;13(4):733. https://doi.org/10.3390/sym13040733.
34. Di Marco G, Gismondi A, Canuti L, Scimeca M, Volpe A, Canini A. Tetracycline accumulates in *Iberis sempervirens* L. through apoplastic transport

inducing oxidative stress and growth inhibition. Plant Biol. 2014;16(4):792. https://doi.org/10.1111/plb.12102.
35. Lichtenthaler HK. Chlorophylls and carotenoids: pigments of photosynthetic biomembranes. Methods Enzymol. 1987;148:350. https://doi.org/10.1016/0076-6879(87)48036-1.
36. Duan Y, Zhang W, Li B, Wang Y, Li K, Sodmergen T, Han C, Zhang Y, Li X. An endoplasmic reticulum response pathway mediates programmed cell death of root tip induced by water stress in *Arabidopsis*. New Phytol. 2010;186(3):681. https://doi.org/10.1111/j.1469-8137.2010.03207.x.
37. Gustavino B, Carboni G, Petrillo R, Paoluzzi G, Santovetti E, Rizzoni M. Exposure to 915 MHz radiation induces micronuclei in *Vicia faba* root tips. Mutagenesis. 2016;31(2):187. https://doi.org/10.1093/mutage/gev071.
38. Heath RL, Packer L. Photoperoxidation in isolated chloroplasts. I. Kinetics and stoichiometry of fatty acid peroxidation. Arch Biochem Biophys. 1968;125(1):189. https://doi.org/10.1016/0003-9861(68)90654-1.
39. De Rossi S, Di Marco G, Bruno L, Gismondi A, Canini A. Investigating the drought and salinity effect on the redox components of *Sulla coronaria* (L.) Medik. Antioxidants. 2021;10(07):1048. https://doi.org/10.3390/antiox10071048.
40. Wohlgemuth H, Mittelstrass K, Kschieschan S, Bender J, Weigel HJ, Overmyer K, Kangasjärvi J, Sandermann H, Langebartels C. Activation of an oxidative burst is a general feature of sensitive plants exposed to the air pollutant ozone. Plan Cell Environ. 2002;25(6):717. https://doi.org/10.1046/j.1365-3040.2002.00859.x.
41. Rodríguez-Serrano M, Romero-Puertas MC, Zabalza A, Corpas FJ, Gómez M, Del Río LA, Sandalio LM. Cadmium effect on oxidative metabolism of pea (*Pisum sativum* L.) roots imaging of reactive oxygen species and nitric oxide accumulation in vivo. Plant Cell Environ. 2006;29(8):1532. https://doi.org/10.1111/j.1365-3040.2006.01531.x.
42. Novelli S, Gismondi A, Di Marco G, Canuti L, Nanni V, Canini A. Plant defense factors involved in *Olea europaea* resistance against *Xylella fastidiosa* infection. J Plant Res. 2019;132(3):439. https://doi.org/10.1007/s10265-019-01108-8.
43. Livak KJ, Schmittgen TD. Analysis of relative gene expression data using real-time quantitative PCR and the 2−ΔΔCT method. Methods. 2001;25(4):402. https://doi.org/10.1006/meth.2001.1262.
44. Tuteja JH, Clough SJ, Chan WC, Vodkin LO. Tissue-specific gene silencing mediated by a naturally occurring chalcone synthase gene cluster in *Glycine max*. Plant Cell. 2004;16(4):819. https://doi.org/10.1105/tpc.021352.
45. Bazin J, Khan GA, Combier JP, Bustos-Sanmamed P, Debernardi JM, Rodriguez R, Sorin C, Palatnik J, Hartmann C, Crespi M, Lelandais-Brière C. miR396 affects mycorrhization and root meristem activity in the legume *Medicago truncatula*. Plant J. 2013;74(6):920. https://doi.org/10.1111/tpj.12178.
46. Bauer EM, Bogliardi G, Ricci C, Cecchetti D, De Caro T, Sennato S, Nucara A, Carbone M. Syntheses of APTMS-coated ZnO: an investigation towards penconazole detection. Materials. 2022;15(22):8050. https://doi.org/10.3390/ma15228050.
47. Handore K, Bhavsar S, Horne A, Chhattise P, Mohite K, Ambekar J, Pande N, Chabukswar V. Novel green route of synthesis of ZnO nanoparticles by using natural biodegradable polymer and its application as a catalyst for oxidation of aldehydes. J Macromol Sci A. 2014;51(12):941. https://doi.org/10.1080/10601325.2014.967078.
48. Winiarski J, Tylus W, Winiarska K, Szczygieł I, Szczygieł B. XPS and FT-IR characterization of selected synthetic corrosion products of zinc expected in neutral environment containing chloride ions. J Spectrosc. 2018. https://doi.org/10.1155/2018/2079278.
49. Musić S, Popović S, Maljković M, Dragčević D. Influence of synthesis procedure on the formation and properties of zinc oxide. J Alloy Compd. 2002;347(1–2):324. https://doi.org/10.1016/S0925-8388(02)00792-2.
50. Akram W, Garud N. Optimization of inulin production process parameters using response surface methodology. Fut J Pharm Sci. 2020;6(1):1. https://doi.org/10.1186/s43094-020-00087-1.
51. Salavati-Niasari M, Gholami-Daghian M, Esmaeili-Zare M, Sangsefidi FS. Solid state synthesis and characterization of zinc oxide (ZnO) microflakes by [bis (acetylacetonato) zinc (II)] and sodium hydroxide at room temperature. J Clust Sci. 2013;24:1093. https://doi.org/10.1007/s10876-013-0600-5.
52. Mishra B, McDonald LM, Roy M, Lanzirotti A, Myneni SCB. Uptake and speciation of zinc in edible plants grown in smelter contaminated soils. PLoS ONE. 2020;15(4):e0226180. https://doi.org/10.1371/journal.pone.0226180.
53. Miller G, Schlauch K, Tam R, Cortes D, Torres MA, Shulaev V, Dangl JL, Mittler R. The plant NADPH oxidase RBOHD mediates rapid systemic signaling in response to diverse stimuli. Sci Signal. 2009;2(84):45. https://doi.org/10.1126/scisignal.2000448.
54. Sharma I, Ahmad P. Catalase: a versatile antioxidant in plants. In: Ahmad P, editor. Oxidative damage to plants. Cambridge: Academic Press; 2014. p. 131. https://doi.org/10.1016/B978-0-12-799963-0.00004-6.
55. Joubès J, Chevalier C, Dudits D, Heberle-Bors E, Inzé D, Umeda M, Renaudin JP. CDK-related protein kinases in plants. Plant Cell Cycle. 2000. https://doi.org/10.1023/a:1006470301554.
56. Pullagurala VLR, Adisa IO, Rawat S, Kim B, Barrios AC, Medina-Velo IA, Hernandez-Viezcas JA, Peralta-Videa JR, Gardea-Torresdey JL. Finding the conditions for the beneficial use of ZnO nanoparticles towards plants-A review. Environ Pollut. 2018;241:1175. https://doi.org/10.1016/j.envpol.2018.06.036.
57. Hanif S, Sajjad A, Zia M. Proline coated ZnO NPs as nanofertilizer against drought stress: an in vitro study to *Coriandrum sativum*. Plant Cell Tiss Org. 2023. https://doi.org/10.1007/s11240-023-02504-8.
58. Singh NB, Amist N, Yadav K, Singh D, Pandey JK, Singh SC. Impact of nano ZnO on metabolic attributes and fluorescence kinetics of rice seedlings. J Nanoengin Nanomanufact. 2013;3:353. https://doi.org/10.1016/j.enmm.2017.11.006.
59. Wang XP, Li QQ, Pei ZM, Wang SC. Effects of zinc oxide nanoparticles on the growth, photosynthetic traits, and antioxidative enzymes in tomato plants. Biol Plantarum. 2018;62:801. https://doi.org/10.1007/s10535-018-0813-4.
60. Jayarambabu N, Kumari BS, Rao KV, Prabhu YT. Beneficial role of zinc oxide nanoparticles on green crop production. Int J Multidisc Adv Res Trends. 2015;10:273.
61. Itroutwar PD, Kasivelu G, Raguraman V, Malaichamy K, Sevathapandian SK. Effects of biogenetic zinc oxide nanoparticles on seed germination and seedling vigor of maize (*Zea mays*). Biocatal Agricul Biotechn. 2020;29:101778. https://doi.org/10.1016/j.bcab.2020.101778.
62. Pérez-de-Luque A. Interaction of nanomaterials with plants: what do we need for real applications in agriculture? Front Environ Sci. 2017;5:12. https://doi.org/10.3389/fenvs.2017.00012.
63. Bolouri-Moghaddam MR, Le Roy K, Xiang L, Rolland F, Van den Ende W. Sugar signaling and antioxidant network connections in plant cells. FEBS J. 2010;277:2022. https://doi.org/10.1111/j.1742-4658.2010.07633.x.
64. Janse van Rensburg HC, Takács Z, Freynschlag F, Toksoy Öner E, Jonak C, Van den Ende W. Fructans prime ROS dynamics and *Botrytis cinerea* resistance in *Arabidopsis*. Antioxidants. 2020;9(9):805. https://doi.org/10.3390/antiox9090805.
65. Aquilano K, Baldelli S, Rotilio G, Ciriolo MR. Role of nitric oxide synthases in Parkinson's disease: a review on the antioxidant and anti-inflammatory activity of polyphenols. Neurochem Res. 2008;33:2416. https://doi.org/10.1007/s11064-008-9697-6.
66. Hashemi S, Asrar Z, Pourseyedi S, Nadernejad N. Plant-mediated synthesis of zinc oxide nano-particles and their effect on growth, lipid peroxidation and hydrogen peroxide contents in soybean. Indian J Plant Physi. 2016;21:312. https://doi.org/10.1007/s40502-016-0242-3.
67. Livanos P, Apostolakos P, Galatis B. Plant cell division: ROS homeostasis is required. Plant Signal Behav. 2012;7:771. https://doi.org/10.4161/psb.20530.
68. Morales M, Munné-Bosch S. Malondialdehyde: facts and artifacts. Plant Physiol. 2019;180:1246. https://doi.org/10.1104/pp.19.00405.

Publisher's Note